ACS APPLIED MATERIALS & INTERFACES

www.acsami.org

Research Article

Light-Emitting Atomically Precise Nanocluster-Based Flexible QR Codes for Anticounterfeiting

Jose V. Rival, Paloli Mymoona, Rajendran Vinoth, A. M. Vinu Mohan, and Edakkattuparambil Sidharth Shibu*

Cite This: *ACS Appl. Mater. Interfaces* 2021, 13, 10583−10593

Read Online

ACCESS | Metrics & More | Article Recommendations | Supporting Information

ABSTRACT: Despite tremendous progress in the field of fluorescence-based anticounterfeiting, the advanced anticounterfeiting techniques are still posing challenges all over the world due to their cost and reliability. Recently, light-emitting atomically precise nanoclusters have emerged as attractive building blocks because of their well-defined structure, function, and stable photoluminescence. Herein, we report the room temperature fabrication of a stable, flexible, nontoxic, and low-cost precision nanocluster-based luminescent ink for the stencil printing of an optically unclonable security label. Nanocluster-based printing ink shows brilliant photoluminescence owing to its extended C−H···π/π···π interactions. Spectroscopic and microscopic investigations show that intercalated nanoclusters in the printed security labels are highly stable as their optical features and molecular compositions are unaffected. The exceptional mechanical, thermal, photo, and aqueous stabilities of the printed security labels endorse to demonstrate the printing and smartphone-based electronic reading of the quick response code on a currency. Finally, confidential information protection and decryption under a precise window of light have been achieved by adopting the optical contrast illusion. The overall cost of the security label is found to be approximately 0.013 USD per stamp.

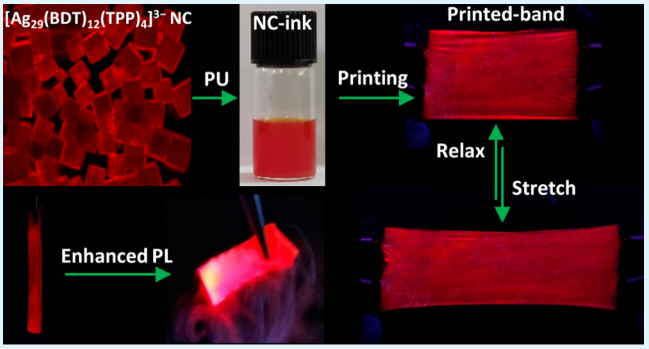

KEYWORDS: *light-emitting nanoclusters, luminescent inks, stencil printing, self-assembly, flexible QR codes, anticounterfeiting, optical contrast illusion*

INTRODUCTION

Counterfeiting of any official documents, especially currency, passport, stamp, and so forth, is a global concern that affects the security and revenue of a country. Although many of these are protected with anticounterfeiting techniques, the estimated global economic loss due to duplication has been increased significantly and reached up to multibillion USD per annum.[1] Conventional anticounterfeiting technology is mainly based on the printing of a security label using an ink developed from luminescent materials that can glow under ultraviolet light. Different materials used or proposed to fabricate the printing ink include organic dyes,[2−6] semiconductor quantum dots,[7−9] inorganic perovskites,[10,11] rare-earth metals,[12−16] upconversion nanoparticles,[17] carbon dots,[18,19] polymer dots,[20] and so on. However, the moderate photostability, sizable elemental toxicity, expensive precursors, or hard synthetic protocols rarely limit their attention. Nontoxic luminescent ink fabricated from the atomically precise nanocluster (NC) is another possible candidate. In the recent past, an attempt to make the NC-based luminescent printing ink was reported.[21] NCs have been considered as a class of materials made up of about ten to a few hundred atoms in their cores.[22,23] Precise atomic combinations, discrete electronic energy levels, characteristic optical absorption features, bright photoluminescence (PL), stability under a range of chemicals and photons, and moderate toxicity due to less metallic contents are the strengths of individual NCs.[24,25] NCs are known for diverse potential applications, which include catalysis,[26,27] solar energy conversion,[28,29] light-emitting diode (LED) fabrication,[30,31] sensing,[32−35] bioimaging,[36−39] drug screening,[40] and therapeutics.[41,42] A large variety of gold and silver NCs with different combinations of cores and ligands are reported.[23−25,43−53] Some of these NCs emit in the solid-state owing to their strong interparticle electronic coupling.[52,53] Stable solid-state emitting NCs with better PL quantum yield are promising materials for developing large-area printable electronics, mainly for security prints, wearable LEDs, and

Received: November 28, 2020
Accepted: February 1, 2021
Published: February 16, 2021

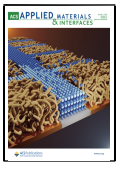

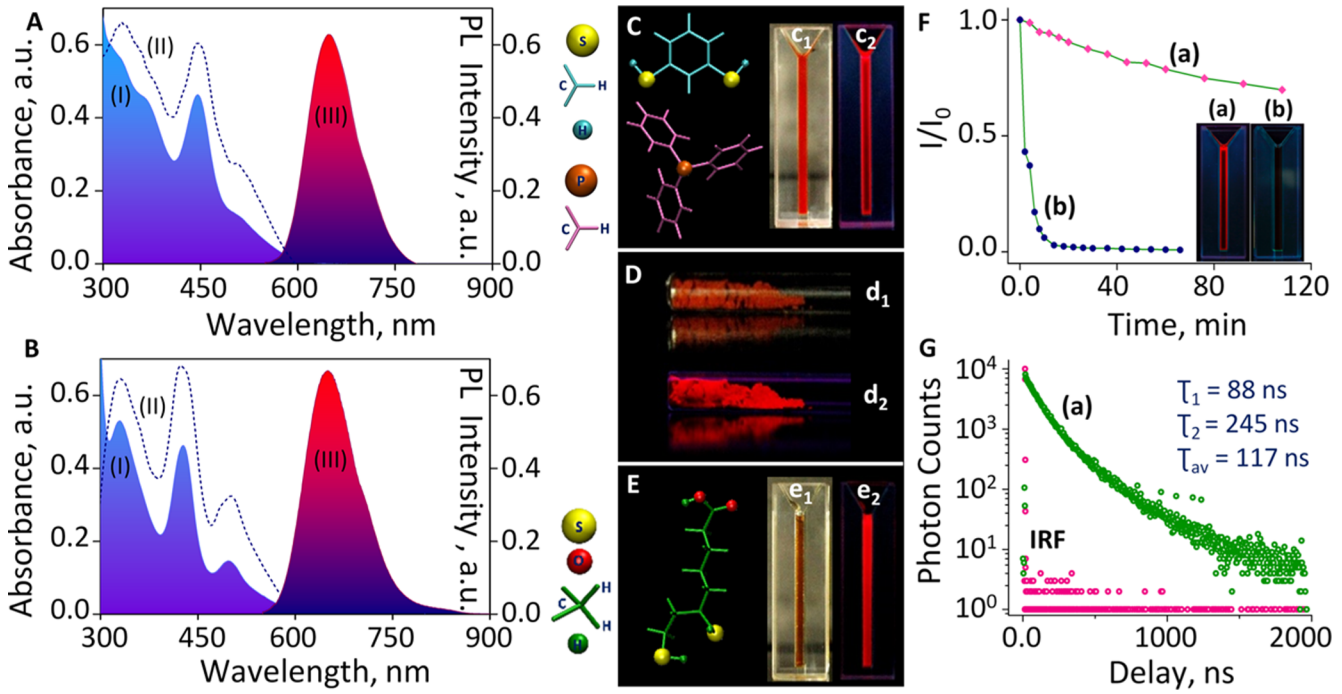

Figure 1. (A,B) UV/vis absorption (I), excitation (II), and PL (III) spectra of (A) $[Ag_{29}(BDT)_{12}(TPP)_4]^{3-}$ and (B) $[Ag_{29}(LA)_{12}]^{3-}$ NCs. (C,E) Photographs of (C) $[Ag_{29}(BDT)_{12}(TPP)_4]^{3-}$ and (E) $[Ag_{29}(LA)_{12}]^{3-}$ NC solutions under visible (c_1 and e_1) and UV light (c_2 and e_2). Energy-minimized structures of the ligands used to synthesize NCs are shown. (D) Photographs of the solid $[Ag_{29}(BDT)_{12}(TPP)_4]^{3-}$ NC under visible (d_1) and UV (d_2) light. (F) Plot of I/I_0 vs illumination time for (a) $[Ag_{29}(BDT)_{12}(TPP)_4]^{3-}$ and (b) $[Ag_{29}(LA)_{12}]^{3-}$ NCs shows their photostability. The photographs (under UV light) of illuminated NC solutions are given in the inset. The PL decay profile of (a) $[Ag_{29}(BDT)_{12}(TPP)_4]^{3-}$ NC and instrument response factor (IRF) are shown in (G).

healthcare sensors. To achieve this goal, the key criterion is to fabricate a smart luminescent NC-based ink having adequate consistency for printing, preserved PL and molecular stability, and flexibility for multiple usages. The development of such a NC-based luminescent printing ink is still in its infancy. To address this challenge, we have fabricated a stable, flexible, nontoxic, and low-cost NC-based luminescent ink by integrating solid-state emitting NCs in an elastic matrix. Different spectroscopic and microscopic studies show that intercalated NCs in the printing ink are highly stable as their optical absorption features, PL, and molecular compositions are analogue to the pristine NCs. This elastic ink has been efficiently used to print the text and quick response (QR) code using the stencil printing technique. A QR code is a machine-readable two-dimensional barcode, which can encrypt data such as name, uniform resource locator (URL), address, phone number, location details, and so on. The information encoded on these optical labels can be accessed by scanning with a camera-enabled mobile device having a QR code scanner application. In the recent past, the QR code fabricated from upconversion nanoparticle-based ink has been used to demonstrate the pharmaceutical anticounterfeiting.[54] Herein, we have successfully demonstrated the printing and electronic reading of a QR code encrypted with "confidential information" on a currency. Notably, the printed security labels are stable over a range of temperatures, under a spectrum of lights, humidity, and mechanical stress. The elastomeric binder-based luminescent ink facilitates flexible and stretchable solid-state patterns, which helps to hold the printed security code on the currency even after multiple folding and wetting. Using this stretchable luminescent ink, we can print any authentic security codes (2.5 cm × 2.5 cm) at the cost of 0.013 USD per stamp. This methodology can be further extended to encrypt more details about the currency, such as serial numbers, or any other pieces of information to validate its authenticity.

RESULTS AND DISCUSSION

To address the development of a stable, nontoxic, and low-cost NC-based luminescent ink, different gold and silver NCs were scrutinized. Among these, twenty-nine-atom silver NCs (Ag_{29}) have been selected to fabricate the printing ink. Details are provided in the Supporting Information (Figure S1). Two different Ag_{29} NCs, viz, $[Ag_{29}(BDT)_{12}(TPP)_4]^{3-}$ and $[Ag_{29}(LA)_{12}]^{3-}$, were synthesized and purified according to protocols reported elsewhere.[53,55] Details are given in the Experimental Section. Both of these NCs were characterized using optical absorption and PL spectroscopy. Figure 1A,B shows the UV/vis absorption (I), excitation (II), and PL (III) spectra of $[Ag_{29}(BDT)_{12}(TPP)_4]^{3-}$ and $[Ag_{29}(LA)_{12}]^{3-}$ NCs in *N*,*N*-dimethylformamide (DMF). Different absorption humps, *ca.* 265, 365, 445, and 510 nm, represent different possible molecular electronic transitions, which are more prominent in the excitation spectra. PL spectra of these NCs show an emission maximum *ca.* 650 nm at 450 nm excitation. Photographs of $[Ag_{29}(BDT)_{12}(TPP)_4]^{3-}$ and $[Ag_{29}(LA)_{12}]^{3-}$ NC solutions under visible (c_1 and e_1) and UV light (c_2 and e_2) and the energy-minimized structure of the ligands used to synthesize NCs are shown in Figure 1C,E, respectively. Among two NCs, $[Ag_{29}(BDT)_{12}(TPP)_4]^{3-}$ shows bright solid-state emission, a fundamental requirement for the luminescent-based printing ink. Photographs of $[Ag_{29}(BDT)_{12}(TPP)_4]^{3-}$ NC powder under visible (d_1) and UV light (d_2) are shown in Figure 1D. To evaluate the photostability of NCs, we have

https://dx.doi.org/10.1021/acsami.0c21127
ACS Appl. Mater. Interfaces 2021, 13, 10583−10593

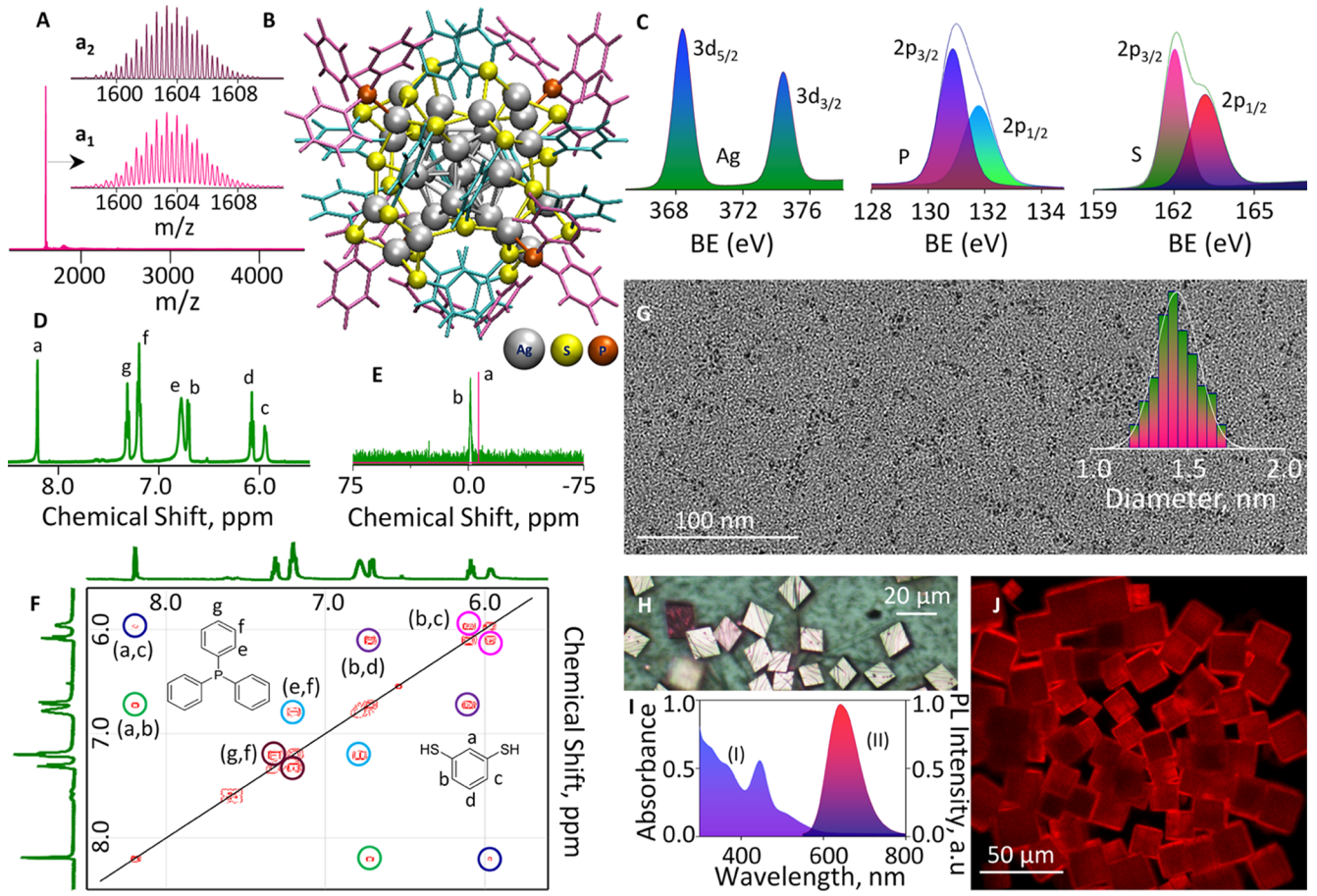

Figure 2. (A,B) ESI-MS and energy-minimized structure of the $[Ag_{29}(BDT)_{12}(TPP)_4]^{3-}$ NC. An expanded view of (a_1) experimental and (a_2) theoretical isotopic patterns are shown in the inset. (C) XPS spectra of the NC show the presence of silver, phosphorus, and sulfur. (D) ^{1}H, (E) ^{31}P, and (F) ^{1}H−^{1}H correlation (COSY) NMR spectra of the $[Ag_{29}(BDT)_{12}(TPP)_4]^{3-}$ NC. All the peaks are assigned and labeled above the traces. (G) Larger area TEM image shows monodisperse NCs. The size distribution of the NC is shown in the inset. (H,J) Optical and confocal fluorescence images of the crystallized NC show rhombohedral crystals. (I) Absorption (I) and PL (II) spectra of redissolved crystals recorded in DMF.

recorded and compared the time-dependent PL spectra of $[Ag_{29}(BDT)_{12}(TPP)_4]^{3-}$ and $[Ag_{29}(LA)_{12}]^{3-}$ NC solutions illuminated at 365 nm excitation at different time intervals. Photostability experiments show extended stability for $[Ag_{29}(BDT)_{12}(TPP)_4]^{3-}$ NCs compared to $[Ag_{29}(LA)_{12}]^{3-}$ NCs (Figure 1F). Illumination of $[Ag_{29}(LA)_{12}]^{3-}$ NC solution (365 nm light) underwent photobleaching within 15 min, which is evident from the plot of (b) I/I_0 vs illumination time (I_0 represents the PL intensity at $t = 0$). At the same time, the $[Ag_{29}(BDT)_{12}(TPP)_4]^{3-}$ NC shows (a) robust I/I_0 values even for a couple of hours of photoexcitation. The photographs (under UV light) of (a) $[Ag_{29}(BDT)_{12}(TPP)_4]^{3-}$ and (b) $[Ag_{29}(LA)_{12}]^{3-}$ NC solutions illuminated under 365 nm light are given in the inset (Figure 1F). Temporal PL spectra recorded from both of these NCs under 365 nm illumination are given in the Supporting Information (Figure S2). Due to the exceptional photostability, easy synthetic protocol, solid-state emission, and less cost of raw materials, we have chosen $[Ag_{29}(BDT)_{12}(TPP)_4]^{3-}$ as the potential ingredient for the fabrication of luminescent ink. Before that, a comprehensive picture of $[Ag_{29}(BDT)_{12}(TPP)_4]^{3-}$ NCs was investigated in detail using various spectroscopic and microscopic techniques. The PL lifetime of $[Ag_{29}(BDT)_{12}(TPP)_4]^{3-}$ NC solution was recorded using time-resolved spectroscopy. Figure 1G (a) represents the PL decay profile (time-correlated single-photon counting, TCSPC) of the NC at its emission maximum *ca.* 650 nm using 378 nm excitation. The $[Ag_{29}(BDT)_{12}(TPP)_4]^{3-}$ NC shows a biexponential luminescence relaxation with a faster component of 88 ns and a slower component of 245 ns. The fast and slow components of NCs presumably originated from the prompt and thermally activated delayed emission, similar to the other NCs reported.[39,56] The average lifetime of NC is found to be 117 ns,[57] which was estimated using the equation $\tau_{av} = (\tau_1 A_1 + \tau_2 A_2)/(A_1 + A_2)$, where τ_1 and τ_2 are the individual lifetime values and A_1 and A_2 are the corresponding amplitudes.

The molecular composition of $[Ag_{29}(BDT)_{12}(TPP)_4]^{3-}$ NC was recorded and analyzed using electrospray ionization-mass spectrometry (ESI-MS, negative mode). ESI-MS of the purified $[Ag_{29}(BDT)_{12}(TPP)_4]^{3-}$ NC in DMF is shown in Figure 2A, which is comparable to the reported spectrum.[53,57] Single molecular ion peak *ca.* 1603 represents pure $[Ag_{29}(BDT)_{12}]^{3-}$. The molecular weight of TPP is not accounted in the mass spectrum owing to its easy dissociation during ionization.[57] Expansion of the peak *ca.* 1603 shows the characteristic isotopic distribution, in which separation between nearby peaks is found to be 0.33 (inset in Figure 2A, a_1). The corresponding theoretical isotopic distribution is shown in the inset (Figure 2A, a_2). The structure of the $[Ag_{29}(BDT)_{12}(TPP)_4]^{3-}$ NC consists of a Ag_{13} icosahedral

https://dx.doi.org/10.1021/acsami.0c21127
ACS Appl. Mater. Interfaces 2021, 13, 10583−10593

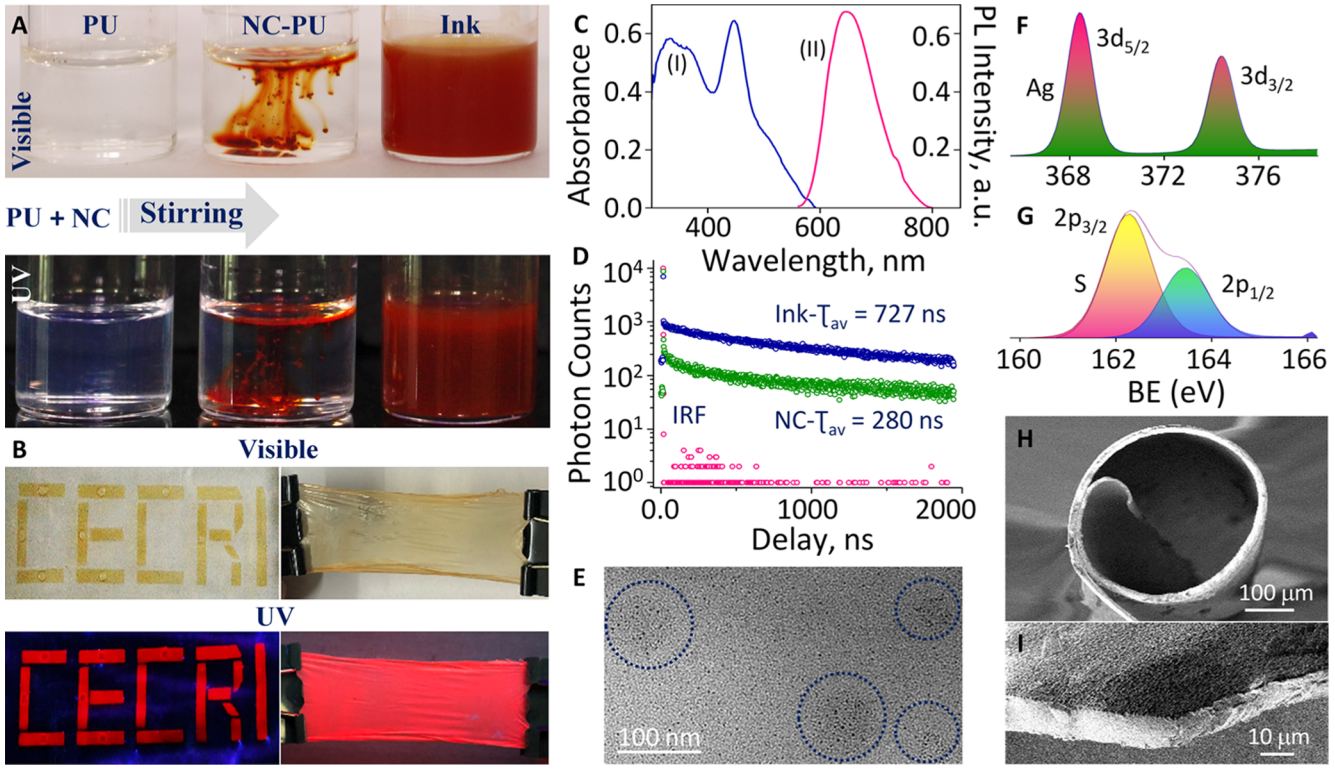

Figure 3. Photographs represent (A) different steps involved in the fabrication of ink and (B) stencil-printed luminescent word (CECRI) and band under visible and UV light. (C) UV/vis absorption (I) and PL (II) spectra, (D) PL decay profile, (E) TEM image, and (F,G) XPS spectra (Ag 3d and S 2p) recorded from the luminescent ink/band. Peaks are assigned and labeled above the traces. (H,I) FESEM images taken from the (H) rolled and (I) flat printed band.

core with 12 Ag atoms capped in the external shell. These twelve Ag atoms form four tetrahedrally oriented trigonal prisms, and another four Ag atoms face-cap the thirteen-atom core at four tetrahedral positions.[53] The energy-minimized structure of $[Ag_{29}(BDT)_{12}(TPP)_4]^{3-}$ NC optimized using the density functional theory (DFT) is shown in Figure 2B. The core of the NC and the nature of binding were studied by recording and analyzing the X-ray photoelectron spectrum. Binding energy (BE) values of Ag 3d levels in the $[Ag_{29}(BDT)_{12}(TPP)_4]^{3-}$ NC are in good agreement with reported values,[57,58] with Ag $3d_{5/2}$ *ca.* 368.4 eV and Ag $3d_{3/2}$ *ca.* 374.4 eV (Figure 2C). The deconvoluted spectrum shows the presence of P $2p_{3/2}$ and $2p_{1/2}$ peaks *ca.* 130.8 and 131.8 eV, which confirm the presence of bound TPP in the NC. The BE of S 2p was in accordance with thiolate binding, in which sulfur $2p_{3/2}$ and $2p_{1/2}$ peaks appear around 162 and 163.2 eV, respectively. By comparing ESI-MS and X-ray photoelectron spectroscopy (XPS), the molecular composition of the $[Ag_{29}(BDT)_{12}(TPP)_4]^{3-}$ NC is confirmed.

To further confirm the presence of bound ligands in the purified NC, we have recorded and analyzed ^1H and ^{31}P nuclear magnetic resonance (NMR) spectra in DMSO-d_6. ^1H and ^{31}P NMR spectra of $[Ag_{29}(BDT)_{12}(TPP)_4]^{3-}$ NC solution were assigned and labeled (Figure 2D,E), by comparing the proton−proton interactions in the correlation NMR (COSY; Figure 2F). The peaks *ca.* δ = 8.22−8.20, 6.72−6.69, 6.10−6.05, and 5.98−5.92 ppm were assigned to BDT, whereas the other peaks (δ = 7.34−7.29, 7.24−7.16, and 6.84−6.74) were originated from TPP. The proton in between the thiol groups (Figure 2D, a) has shown a downfield shift owing to the electron-withdrawing nature of the silver core. The environmental changes around NCs resulted in two different sets of peaks for identical protons (Figure 2D, b and c). Appearance of all the aromatic protons in ^1H NMR and a single broad peak (Figure 2E, b) *ca.* −1.44 ppm (slight changes will be expected according to the TPP amount present) in ^{31}P NMR suggests the presence of bound BDT and TPP in the purified NC.[57,59] A small hump *ca.* 25.6 ppm (Figure 2E, b) arises from the oxidized TPP due to air oxidation of NCs.[60] The ^{31}P NMR spectrum of the parent TPP molecule shows a single narrow peak *ca.* −6.818 ppm (Figure 2E, a). The NC was further characterized using transmission electron microscopy (TEM) by drop-casting and drying ∼100 μM solution of the $[Ag_{29}(BDT)_{12}(TPP)_4]^{3-}$ NC in DMF on a copper grid with a carbon-supported film. The TEM image (Figure 2G) shows nearly uniform size distribution (1.5 ± 0.2 nm; inset in Figure 2G) in the grid, which indicates the monodispersity of the $[Ag_{29}(BDT)_{12}(TPP)_4]^{3-}$ NC. As an extreme purity is recommended in the printing gadgets, NCs were further purified by the crystallization using a slow solvent evaporation technique.[53] Optical (white light) and confocal fluorescence images of rhombohedral crystals are shown in Figure 2H,J, respectively. Resemblances in the optical absorption (I) and PL (II) features (Figure 2I) of NC crystals redissolved in DMF verify the Ag_{29} core.

To develop a flexible NC-based printing ink, we have chosen thermoplastic polyurethane (PU) polymer as a matrix to intercalate NCs. The elastic and transparent natures of PU help to adopt the flexibility and visibility for NC-based ink. Details of ink preparation are given in the Experimental Section. Photographs (under visible and UV light) demonstrating the different steps involved in the fabrication of NC-

https://dx.doi.org/10.1021/acsami.0c21127
ACS Appl. Mater. Interfaces 2021, 13, 10583−10593

based ink are shown in Figure 3A. The addition of crystallized NCs into the PU dispersion previously prepared in tetrahydrofuran (THF) followed by constant stirring at room temperature ensured high-quality printing ink with the required consistency. To check the competence of the above-prepared ink, we have printed luminescent letters and bands using a stencil printing technique.[61−64] Details are provided in the Experimental Section. Figure 3B shows the photographs (under visible and UV light) of a word (CECRI) and a band stencil-printed on a tattoo paper. The perfect texture of the ink helped to print the letters without any diffusion. Moreover, the printed band is highly transparent, which allows us to see the background (Figure S3). To ensure the stability of NCs in the printed patterns, their optical features were probed using different spectroscopic and microscopic techniques. One-to-one correspondence in the UV/vis absorption (I) and PL (II) spectra recorded from the printed band (Figure 3C) with Figure 1A suggests that NCs are stable in ink and in the printed patterns. The PL decay profile (TCSPC) recorded from the printed band (378 nm excitation) shows a prolonged lifetime (727 ns; Figure 3D) compared to the parent NC crystals (280 ns) due to their least collisional quenching in the excited state. The longer lifetime of NCs in the printed band rules out their direct interactions with atmospheric oxygen because of the polymer coating. Subsequently, we have investigated the morphology of NCs in the printed band by recording and analyzing the TEM images of ink coated on a carbon-supported copper grid. The TEM image of NCs dispersed in ink or printed band is shown in Figure 3E, which suggests the unaltered size of NCs. However, we could observe random organization of NCs in the grid, marked by blue circles. Detailed TEM investigation shows a circular assembly of NCs in the polymer matrix (Figure S4A). Such an organization is mostly due to the C−H···π/π···π interactions between the BDT/TPP and PU moieties, similar to the assembly reported in $[Ag_{29}(BDT)_{12}(TPP)_4]^{3-}$ NCs.[65] Furthermore, we have recorded and compared the PL spectra of an equimolar concentration of parent NCs and ink. Notably, the PL spectrum recorded from the ink shows fourfold enhancement compared to the NC solution (Figure S4B) under similar experimental conditions. The enhanced PL and extended lifetime of NCs in ink and the printed band seemingly originated from their assembly. The earlier reports on the self-organization of NCs in a polymer matrix[66] and enhanced PL in the assembled NCs[66,67] support the above-mentioned results. The XPS spectra recorded and analyzed from the printed band provided BE values of Ag 3d (Figure 3F; Ag $3d_{5/2}$ *ca.* 368.4 eV and $3d_{3/2}$ *ca.* 374.4 eV) and S 2p (Figure 3G; S $2p_{3/2}$ *ca.* 162.3 eV and $2p_{1/2}$ *ca.* 163.5 eV), which are in good agreement with pristine NCs[57,58] (Figure 2C). Slight broadening in the BE of P 2p (Figure S5A) is probably due to the presence of unbound[57] or oxidized TPP[60] in the film. Although a small amount of TPP separated from the NC surface during the ink fabrication, NCs were found to be highly stable in ink. The XPS spectra representing the BE of O 1s and N 1s (polymer) are shown in Figure S5B,C, respectively. The thickness of the printed materials is essential, especially in high-security documents. To measure the thickness of the printed band, we have recorded and analyzed scanning electron microscopy (SEM) micrographs. Field emission (FE) SEM images of the printed band captured from different areas are given in Figure 3H (rolled) and I (flat), which show nearly uniform thickness (~8.75 ± 0.85 μm) and surface morphology. The elemental composition of the printed band is given in the Supporting Information (Figure S6). All the abovementioned experiments confirm the presence of stable NCs in ink and in the printed bands.

Stability of the printed materials is indispensable, especially for the authorized documents. We have systematically investigated photostability, thermal stability, moisture effect, and mechanical strength of the printed bands. To study their photostability, we have recorded and analyzed the PL spectra from the printed band illuminated at 365 nm excitation at different time intervals. A plot of I/I_0 (Figure 4A) vs

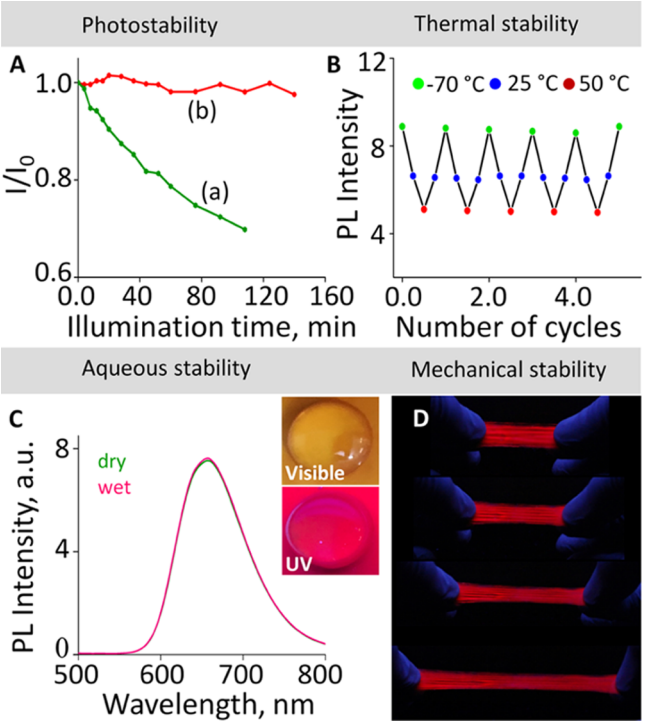

Figure 4. (A) Plot of I/I_0 vs illumination time recorded from (a) NC solution and (b) printed band illuminated at 365 nm. (B) Plot of PL intensity vs number of temperature cycles recorded from the printed band kept at −70, 25, and 50 °C. (C) PL spectra recorded from the printed band under wet and dry conditions. Photographs of a wet band under visible and UV light are shown in the inset. (D) Photographs of the printed band captured during the stretching test under UV light.

illumination time shows an exceptional photostability for (b) NCs embedded in the printed band compared to (a) NC solution (Figure 1F-a) under similar experimental conditions. The temporal PL spectra recorded from the printed band are given in the Supporting Information (Figure S7). To test their thermal stability, PL spectra were recorded from the printed band kept at different temperatures. A range of temperatures from −70 to 50 °C were achieved by soaking the printed band in liquid nitrogen, cold water, and warm water. A plot of PL intensity vs the number of temperature cycles (Figure 4B) shows switchable PL under variable temperatures, which suggests the stability of NCs in the printed band over a range of temperatures. Additionally, the unaltered optical absorption features of NCs (Figure S8A) recorded after dipping the printed band in liquid nitrogen, cold water, and warm water proved the stability of NCs at different temperatures. As expected, PL intensity was maximum at low

https://dx.doi.org/10.1021/acsami.0c21127
ACS Appl. Mater. Interfaces 2021, 13, 10583−10593

temperature owing to the least rotational and vibrational movements of bound ligands on the NC surface. The photograph showing the enhanced PL from the printed band while dipping in liquid nitrogen is shown in the Supporting Information (Figure S8C). Five cycles of PL spectra recorded from the printed band soaked at different temperatures are provided in the Supporting Information (Figure S9). The abovementioned set of the experiment also suggests the durability of printed materials in a wet environment. To further study the moisture effect, we have recorded and compared the PL spectra of the printed band after wetting (Figure 4C). The analogue PL spectra recorded from the printed band under dry and wet conditions confirm their stability in humid settings. Photographs of a wet band under visible and UV lights (inset in Figure 4C) show their hydrophobicity, which was further confirmed by contact angle measurements. Details are provided in the Experimental Section. The water drop profile used to determine the water contact angle on the printed band is shown in Figure S10. The measured contact angle from the NC−PU printed band (93.72 ± 0.85°) is comparable to the PU-alone printed band (95.78 ± 0.5°). A slight decrease in the contact angle of the NC−PU printed band is attributed to the polar nature of NCs. The integrity of NCs in the printed band was tested by keeping them in a water (Millipore) bath for a long time. A robust PL from the printed band showed exceptional stability of NCs in water (Figure S11).

Furthermore, we have tested the elasticity of the printed free-standing band (3 cm × 1 cm × 0.01 mm) by stretching and relaxing them multiple times. Photographs (under UV light) captured during the different sequences of stretching (Figure 4D) and wincing (Figure S12A) demonstrate the flexibility and mechanical strength of the printed bands. We also tested the restoring ability of the printed band after stretching. The photographs captured before and after the stretching are shown in Figure S12B. This suggests a nearly complete recovery in the size and shape of the printed band. Later, tensile strength and elongation at the breaking point of the printed band were tested and compared with the PU band. The stress−strain curve recorded from the NC−PU and PU-alone printed bands are shown in the Supporting Information (Figure S13). The tensile strength of the NC−PU band was slightly decreased from 28.4 ± 2.1 to 25.32 ± 0.6 MPa. This could probably be due to the molecular interactions between NCs and PU moieties discussed earlier. The NC−PU band withstood 229 ± 16% strain, comparable to the PU band (253 ± 10%). All the abovementioned spectroscopic information suggests that NC in ink is stable and reliable to print any relevant documents.

Proven after the stability of NC-based luminescent ink, we have further employed them to fabricate an electronic security label on the currency. The schematic representation of the stencil printing technique used to print a static QR code is shown in Figure 5A. The QR code-stencil pattern previously encrypted with the "confidential information" has been used to print security labels. The photographs (under visible and UV light) of a QR code-printed on an A4 paper are provided in the Supporting Information (Figure S14A,B). Here, the blue background (under UV light) is because of the fluorescence coming from the optical brightener (OB) used in the paper. As a result, the red emission of the NC was merged with OB emission. Interestingly, we found that the printed QR code is readable only under UV light. This is due to optical contrast illusion created by the combination of blue and red emissions

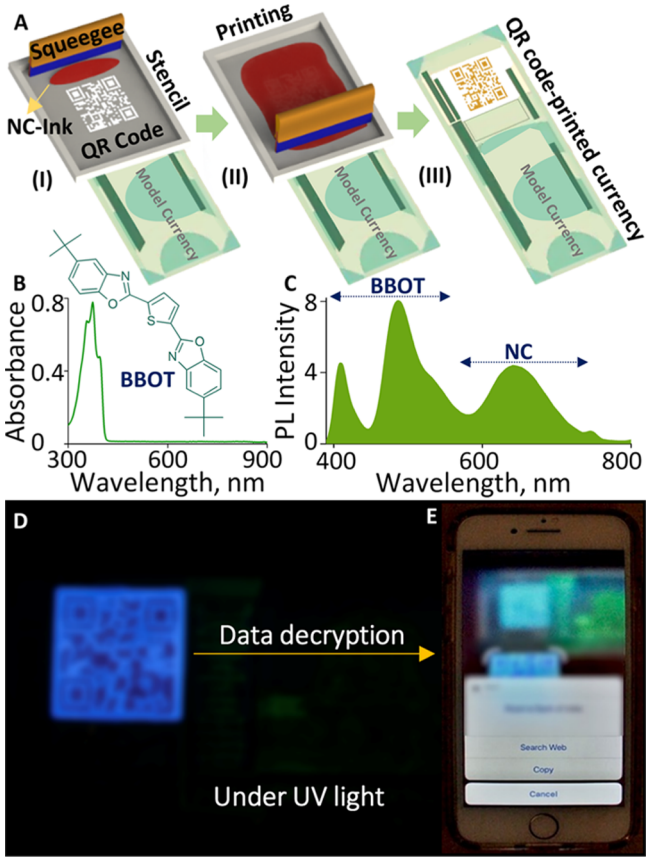

Figure 5. (A) Schematic representation of the stencil printing technique used to print QR code on a currency. (B) Absorption spectrum and chemical structure of BBOT. (C) Combined PL spectrum recorded from a mixture of NCs and BBOT. Photographs of the (D) QR code-printed currency and (E) data decryption process using a smartphone under UV light. The photograph of the QR code-printed original currency has been blurred to avoid copyright issues.

from OB and NCs, respectively. Later, we have extended the same strategy to print high-security QR code on a currency. The raw materials vary from currency to currency during their manufacture. Hence, it is essential to ensure a homogeneous surface on the currency as a background for QR code printing. Also, the QR code recognition and decryption necessitate a significant difference in the background to foreground color contrast. To address such challenges, we have selected thiophene-based OB [2,5-bis-(5-*tert*-butyl-benzoxazol-2-yl)-thiophene (BBOT)], which is extensively used in printed electronics and laser applications. The optical absorption spectrum and chemical structure of BBOT are given in Figure 5B. The better solubility of this molecule in THF helped to make highly uniform BBOT−PU dispersion. An interface layer of BBOT−PU was initially printed on the currency, which helps to ensure uniform surface and durable adhesion of the QR code. Subsequently, the QR code has been printed on top of the BBOT−PU layer using the previously prepared NC-based luminescent ink. Printing details are provided in the Experimental Section. The schematic representation is shown in Figure 5A. The photographs of the QR code-printed currency captured under visible and UV lights are provided in Figures S14C and 5D, respectively. Similar to the previous case, the printed QR code is readable only under UV light. Figure 5E shows the photograph representing the QR code

https://dx.doi.org/10.1021/acsami.0c21127
ACS Appl. Mater. Interfaces 2021, 13, 10583−10593

decryption process using a smartphone. Due to copyright issues, the photographs of the original currency and QR code were blurred. The QR code-printed currency was kept under UV light during the data decryption. The presence of BBOT helped to enhance the optical contrast between the interface layer (BBOT−PU) and the NC layer, which indeed supports the decryption of a security label specifically under UV light. Additionally, the BBOT−PU layer allows facile decryption of the QR codes-printed on any universal currencies preloaded with unspecified UV sensitive interfering inks. Although the combined emission of BBOT and NCs under 365 nm excitation (Figure 5C) reduced the PL brightness of NCs in ink (Figure 5D), we could successfully demonstrate the printing and electronic reading of a QR code on currency via the optical contrast illusion process. The printed security label is optically unclonable as their electronic absorption bands and PL features are highly precise (Figure 3C). Later, we have tested the mechanical stability of the QR code-printed currency by a folding assay. The photographic evidence shows (Figure S15A; under UV light) that the printed security label is stable even after multiple folding. Finally, we have tested aqueous stability of QR code-printed currency by dipping them in water (Figure S15B). The poor solubility of NCs and BBOT in water prevents their leaching. The data decryption was successful after both folding and wetting trials. The exceptional mechanical, thermal, photo, and aqueous stability of the printed documents suggest that NC-based luminescent ink can be further extended to develop the next-level security codes.

CONCLUSIONS

In summary, we have successfully demonstrated the room temperature fabrication of nontoxic, cost-effective, reliable, and optically unclonable luminescent security labels. Such security labels are fabricated through the stencil printing technology using near NIR-emitting precise NCs as the primary component in ink. The successful intercalation of NCs into the PU matrix helped to develop light-emitting and flexible ink. NC-based ink displayed brilliant PL owing to their strong C−H$\cdots\pi/\pi\cdots\pi$ interactions. Spectroscopic and microscopic techniques were employed to study the stability of NCs in ink and the printed band. Robust optical absorption, PL, and molecular composition of NCs suggest their extended stability in ink. Detailed investigation of the printed security labels disclosed their unique mechanical, thermal, photo, and aqueous stability. This information helped to demonstrate the printing and electronic reading of the QR code on a currency using a smartphone. Encryption and decryption of a security label under a defined spectrum of light were demonstrated by creating an optical contrast illusion on the currency. The elastomeric binder helped to hold the printed QR code on currency even after multiple folding and wetting. The overall cost of a security label has been estimated to be approximately 0.013 USD per stamp. The anticounterfeiting technology can be further upgraded by printing the dynamic QR codes that enable us to update the encrypted data even after printing. In the future, this particular low-cost and nontoxic luminescent-based ink can be extended to develop wearable LEDs, healthcare sensors, pharmaceutics, and food technology.

EXPERIMENTAL SECTION

Reagents and Materials. All the chemicals and solvents are of analytical grade and used without any further purification. Silver nitrate ($AgNO_3$), 1,3-benzenedithiol (BDT), sodium borohydride ($NaBH_4$), potassium hydroxide (KOH), BBOT, methanol, acetone, THF, dichloromethane (DCM), DMF, gold(III) chloride trihydrate ($HAuCl_4{\cdot}3H_2O$), glutathione (GSH), 2-phenylethanethiol (PET), *p*-mercaptobenzoic acid (*p*-MBA), tetraoctylammonium bromide (TOAB), toluene, and hydrochloric acid (HCl) were purchased from Sigma-Aldrich. α-Lipoic acid (LA) and triphenylphosphine (TPP) were purchased from Tokyo Chemicals Industry (TCI). Sodium hydroxide (NaOH) and ammonium acetate (NH_4OAc) were purchased from Fisher Scientific. DMSO-d_6 was purchased from Sisco Research Laboratories (SRL). Medical grade thermoplastic PU (TECOFLEX EG-93A) was received from Lubrizol Advanced Materials India.

Characterization. ^{1}H and ^{31}P NMR measurements were carried out using Bruker AVANCE III HD 400/500 MHz spectrometers. UV/vis absorbance spectra were recorded on a Varian Cary 500 Scan spectrometer. PL spectra were recorded using a Horiba Fluorolog 3 spectrometer. The fluorescence lifetime measurements were carried out using a Horiba (model DeltaFlex) TCSPC system. The samples were excited using a 378 nm pulsed diode laser (NanoLED-375L; <100 ps pulse duration). ESI-MS measurements were carried out on a Waters Synapt G2-Si high-definition mass spectrometer. Typical experimental parameters of ESI-MS were as follows: capillary voltage: 3 kV, cone voltage: 20 V, source offset: 20 V, source temperature: 100 °C, desolvation temperature: 150 °C, and desolvation gas flow: 400 L/h. HR-TEM images were recorded on a FEI Talos F200S (200 kV) TEM. FESEM images were recorded using a Carl-Zeiss SUPRA 55VP field emission scanning electron microscope. XPS spectra were recorded using a Thermo Scientific ESCALAB 250Xi (XR6 Micro-focused Monochromator, Al Kα). Optical images of crystalized NCs were recorded using a Horiba Jobin Yvon LabRAM HR Evolution laser Raman microscope. The confocal fluorescence image of crystallized NCs was recorded using a Carl Zeiss-LSM 880 confocal laser scanning microscope (458 nm laser). Surface hydrophobicity of NC−PU and PU-alone films was examined using an AST VCA optima (S/N-1020041134) contact angle analyzer. Distilled water (5 μL/drop) was used to measure the contact angle on NC−PU film-coated surfaces by dispensing water using a motorized syringe at 25 °C. The stress−strain analysis was carried out at room temperature using a universal testing machine (Instron 3366; Instron Crop. USA). The printed band (50 mm length × 10 mm width) was fixed into the testing station and subjected to an extension rate of 10 mm/min. Energy-minimized structures of NCs were optimized using DFT as implemented in the grid-based projector augmented wave (GPAW) software package.[68] The structures were optimized in real space having a grid spacing of 0.2 Å for the electron density with the PBE[69] functional in the FD mode. The convergence criterion for residual forces was set to be 0.05 eV/Å, without imposing any symmetry constraints. The following PAW setups were considered for Ag($4d^{10}5s^1$), S($3s^23p^4$), P($3s^23p^3$), O($2s^22p^4$), C($2s^22p^2$), and H($1s^1$), with scalar-relativistic effects included for Ag. The visual molecular dynamics (VMD) software[70] was used for the visualization of the structures.

Synthesis of $[Ag_{29}(BDT)_{12}(TPP)_4]^{3-}$ NCs. $[Ag_{29}(BDT)_{12}(TPP)_4]^{3-}$ NCs were synthesized using a reported protocol.[53] Briefly, in a glass tube, 13.5 μL of BDT was added to 10 mL of DCM. $AgNO_3$ (20 mg) was separately dissolved in 5 mL of methanol by ultrahigh sonication. The addition of $AgNO_3$ solution into the above-prepared reaction mixture resulted in a turbid yellow solution, indicating the formation of an insoluble silver−thiolate complex. The mixture was cooled to ice-cold temperature. The addition of TPP (200 mg/1 mL DCM) into the turbid yellow solution resulted in the formation of a colorless solution. The reaction mixture was allowed to stir for another 10 min before adding a freshly prepared aqueous ice-cold $NaBH_4$ solution (10.5 mg/500 μL). The color of the solution turned dark brown immediately, which gradually

https://dx.doi.org/10.1021/acsami.0c21127
ACS Appl. Mater. Interfaces 2021, 13, 10583−10593

changed (over a period of 5 h) to dark orange, indicating the formation of Ag_{29} NCs. NCs were purified by the ultrahigh centrifugation method (8000 rpm for 2 min). Residual dark orange NCs were washed several times with ethanol to remove all the unreacted materials. Purified NCs were dried under vacuum and stored at 4 °C for further characterizations. Photographs representing the different stages of NCs synthesis are given in the Supporting Information (Figure S16).

Synthesis of $[Ag_{29}(LA)_{12}]^{3-}$ NCs. $[Ag_{29}(LA)_{12}]^{3-}$ NCs were synthesized using a protocol reported elsewhere.[55] Briefly, an aqueous solution of KOH (1 M) was added to LA (19 mg/1 mL) until it dissolves completely. An aqueous solution of $NaBH_4$ (7 mg/100 μL) was added into the abovementioned lipoate solution and stirred for another 15 min. Followed by this, an aqueous $AgNO_3$ (2.9 mg/200 μL) solution was injected and stirred for 30 min at room temperature. The addition of ice-cold $NaBH_4$ (10 mg/100 μL) solution into the abovementioned reaction mixture resulted in a color change from black to dark orange (over a period of 4 h), indicating the formation of NCs. NCs were purified by adding an equal volume of acetone followed by ultrahigh centrifugation (8000 rpm for 2 min). Furthermore, the residual dark orange supernatant solution was precipitated by adding excess acetone. The precipitate was washed several times with ethanol to remove all the unreacted materials. Purified NCs were dried under vacuum and stored at 4 °C for further characterizations.

Fabrication of Luminescent NC-Based Printing Ink. PU was used as an elastomeric binder for the development of stretch-enduring luminescent printing ink. A typical synthesis of ink consists of mixing crystallized NCs (7 or 40 mg) in PU suspension (24 mL) in a shaker for 30 min, followed by constant stirring for another 5 h. The PU suspension was previously prepared by dispersing PU (2 g) in THF (24 mL) using the ultrasonication (30 min) method, followed by continuous stirring (overnight). Similarly, the BBOT−PU suspension was prepared by dispersing PU (2 g) and BBOT (1.25 mg) in THF (24 mL). To print QR codes, we have used low concentration NC−PU (7 mg NC/24 mL PU) dispersion.

Fabrication of the Printed QR Code. The luminescent ink was manually printed on the desired area of the currency using a stencil printing technique. Initially, a static QR code image encrypted with "confidential information" was generated using free available software (https://www.the-qrcode-generator.com). The stencil pattern corresponding to the QR code image was designed using AutoCAD software. The stencil was created on a polyester sheet (100 μm thickness) by engraving the intended sketch using an electronic cutter (Silhouette Cameo, US). The BBOT−PU interface layer was initially printed (2.5 × 2.5 cm) to facilitate the luminescent ink adhesion on the currency substrate and cured at 65 °C for 20 min in a convection oven. Subsequently, the QR code was patterned by printing the luminescent ink on the BBOT−PU layer and cured at 65 °C for 30 min. The luminescent ink movement over the stencil using a squeegee facilitates printing the QR code pattern on the underlying currency substrate. The freestanding stretchable film was prepared by directly printing the luminescent ink on the temporary transfer paper (tattoo paper). The transfer paper was prepared by coating a water-soluble starch layer on the copier paper (80 gsm).[64] Typically, 55% starch was dispersed in water by heating at 95 °C for 15 min and cross-linked with D-sorbitol (45%) under stirring for 1 h. The cross-linked starch was printed on the paper substrate and cured at 70 °C for 30 min. The process was repeated twice to get the homogenous water-soluble film on the paper substrate. The printed luminescent film on the tattoo paper can be released by moisturizing it for 1 min.

■ ASSOCIATED CONTENT

Supporting Information

The Supporting Information is available free of charge at https://pubs.acs.org/doi/10.1021/acsami.0c21127.

Synthetic procedure for $[Au_{22}(SG)_{18}]$, $[Au_{25}(PET)_{18}]^{-}$, $[Au_{102}(p\text{-MBA})_{44}]$, and $[Au_{144}(PET)_{60}]$ NCs; UV/vis absorption and PL spectra of $[Au_{22}(SG)_{18}]$, $[Au_{25}(PET)_{18}]^{-}$, $[Ag_{29}(LA)_{12}]^{3-}$, $[Ag_{29}(BDT)_{12}(TPP)_4]^{3-}$, $[Au_{102}(p\text{-MBA})_{44}]$, and $[Au_{144}(PET)_{60}]$ NCs; time-dependent PL spectra of $[Ag_{29}(BDT)_{12}(TPP)_4]^{3-}$ and $[Ag_{29}(LA)_{12}]^{3-}$ NCs under 365 nm illumination; photograph shows transparency of the printed band; TEM image and PL spectrum recorded from NC-based ink; XPS spectra of P 2p, O 1s, and N 1s recorded from the printed band; EDAX spectrum and elemental composition of the printed band; temporal-PL spectra recorded from the printed band under 365 nm illumination; UV/vis absorption spectra recorded from the printed band kept at different temperatures; photographs of the printed band under UV light before and after dipping in liquid nitrogen; five cycles of PL spectra recorded from the printed band at different temperatures; water drop profiles on PU-alone and NC−PU printed bands; photographs showing the long-term stability of the printed band under water; photographs of the printed band captured during the wincing under UV light; photographs showing the restoring ability of the printed band after stretching; stress−strain curves recorded from the NC−PU and PU-alone printed band; photographs of the printed QR code on A4 paper under visible and UV light; photograph of QR code-printed currency under visible light; photographs of QR code-printed currency captured during folding and wetting assay under UV light; photographs captured during the synthesis of $[Ag_{29}(BDT)_{12}(TPP)_4]^{3-}$ NC; and references (PDF)

■ AUTHOR INFORMATION

Corresponding Author

Edakkattuparambil Sidharth Shibu − *Smart Materials Lab, Electrochemical Power Sources (ECPS) Division, Council of Scientific and Industrial Research (CSIR)-Central Electrochemical Research Institute (CECRI), Karaikudi 630003, Tamil Nadu, India; Academy of Scientific and Innovative Research (AcSIR)-CSIR, Ghaziabad 201002, Uttar Pradesh, India;* orcid.org/0000-0003-3057-4198; Email: shibuchem@gmail.com, shibues@cecri.res.in

Authors

Jose V. Rival − *Smart Materials Lab, Electrochemical Power Sources (ECPS) Division, Council of Scientific and Industrial Research (CSIR)-Central Electrochemical Research Institute (CECRI), Karaikudi 630003, Tamil Nadu, India; Academy of Scientific and Innovative Research (AcSIR)-CSIR, Ghaziabad 201002, Uttar Pradesh, India;* orcid.org/0000-0001-8120-4109

Paloli Mymoona − *Smart Materials Lab, Electrochemical Power Sources (ECPS) Division, Council of Scientific and Industrial Research (CSIR)-Central Electrochemical Research Institute (CECRI), Karaikudi 630003, Tamil Nadu, India; Academy of Scientific and Innovative Research (AcSIR)-CSIR, Ghaziabad 201002, Uttar Pradesh, India;* orcid.org/0000-0003-2251-6676

Rajendran Vinoth − *Academy of Scientific and Innovative Research (AcSIR)-CSIR, Ghaziabad 201002, Uttar Pradesh, India; Electrodics and Electrocatalysis (EEC) Division, Council of Scientific and Industrial Research (CSIR)-Central Electrochemical Research Institute (CECRI), Karaikudi 630003, Tamil Nadu, India*

A. M. Vinu Mohan − *Academy of Scientific and Innovative Research (AcSIR)-CSIR, Ghaziabad 201002, Uttar Pradesh, India; Electrodics and Electrocatalysis (EEC) Division, Council of Scientific and Industrial Research (CSIR)-Central Electrochemical Research Institute (CECRI), Karaikudi 630003, Tamil Nadu, India;* orcid.org/0000-0002-6335-4426

Complete contact information is available at: https://pubs.acs.org/10.1021/acsami.0c21127

Author Contributions

J.V.R. and P.M. contributed equally. The project was designed and supervised by E.S.S. Nanoclusters and ink were synthesized by J.V.R. and P.M. Stencil printing was designed by A.M.V.M. Stencil printing was performed by R.V. and A.M.V.M. All the spectroscopy and microscopy were performed by J.V.R., P.M., and E.S.S. The manuscript was written through the contributions of all authors. All authors have given approval to the final version of the manuscript.

Funding

This work was supported by the Science and Engineering Research Board (SERB) under the Ramanujan Scheme (SB/S2/RJN-005/2017).

Notes

The authors declare no competing financial interest.

■ ACKNOWLEDGMENTS

E.S.S. thanks the Science and Engineering Research Board (SERB) for the Ramanujan Fellowship (SB/S2/RJN-005/2017). A.M.V.M. thanks the Department of Science and Technology (DST) for the DST-INSPIRE Faculty award (DST/INSPIRE/04/2016/001601). We thank DST Unit of Nanoscience (DST-UNS) and Thematic Unit of Excellence (TUE), IIT Madras, for their support for the measurement of ESI-MS and DFT calculations. The authors thank the central instrumentation facility (CIF), CSIR-CECRI, for instrumentation support. We thank Dr. V. Ganesh (CSIR-CECRI) and Dr. D. K. Pattanayak (CSIR-CECRI) for their support in the contact angle and confocal fluorescence measurements. We thank P. Sriram for his support in digital photography. Dr. N. Kalaiselvi (Director, CSIR-CECRI), Dr. S. Sathiyanarayanan (Head, PPMG, CSIR-CECRI), and Dr. P. Murugan (CSIR-CECRI) are acknowledged for their support. J.V.R. thanks SERB for supporting the research fellowship. P.M. thanks the Council of Scientific and Industrial Research (CSIR) for a junior research fellowship.

■ ABBREVIATIONS

NC, atomically precise noble metal nanocluster
PU, polyurethane
QR, quick response

■ REFERENCES

(1) Organization for Economic Cooperation and Development (OECD)/European Union Intellectual Property Office. *Trade in Counterfeit and Pirated Goods: Mapping the Economic Impact*; OECD Publishing, 2016.

(2) Kishimura, A.; Yamashita, T.; Yamaguchi, K.; Aida, T. Rewritable Phosphorescent Paper by the Control of Competing Kinetic and Thermodynamic Self-Assembling Events. *Nat. Mater.* **2005**, *4*, 546−549.

(3) Ajayaghosh, A.; Thirumalai, K. R. Fluorescent Material for Self-Erasable Writing, Authentic Security Labeling, Currency Counterfeit Prevention and Processes for the Preparation Thereof. U.S. Patent 20,130,209,665 A1, August 2013.

(4) Thirumalai, R.; Mukhopadhyay, R. D.; Praveen, V. K.; Ajayaghosh, A. A Slippery Molecular Assembly Allows Water as a Self-Erasable Security Marker. *Sci. Rep.* **2015**, *5*, 09842.

(5) Ding, L.; Wang, X.-d. Luminescent Oxygen-Sensitive Ink to Produce Highly Secured Anticounterfeiting Labels by Inkjet Printing. *J. Am. Chem. Soc.* **2020**, *142*, 13558−13564.

(6) Tian, W.; Zhang, J.; Yu, J.; Wu, J.; Zhang, J.; He, J.; Wang, F. Phototunable Full-Color Emission of Cellulose-Based Dynamic Fluorescent Materials. *Adv. Funct. Mater.* **2018**, *28*, 1703548.

(7) Liu, Y.; Han, F.; Li, F.; Zhao, Y.; Chen, M.; Xu, Z.; Zheng, X.; Hu, H.; Yao, J.; Guo, T.; Lin, W.; Zheng, Y.; You, B.; Liu, P.; Li, Y.; Qian, L. Inkjet-printed Unclonable Quantum Dot Fluorescent Anti-Counterfeiting Labels with Artificial Intelligence Authentication. *Nat. Commun.* **2019**, *10*, 2409.

(8) Liu, Y.; Li, F.; Xu, Z.; Zheng, C.; Guo, T.; Xie, X.; Qian, L.; Fu, D.; Yan, X. Efficient All-Solution Processed Quantum Dot Light Emitting Diodes Based on Inkjet Printing Technique. *ACS Appl. Mater. Interfaces* **2017**, *9*, 25506−25512.

(9) Yang, P.; Zhang, L.; Kang, D. J.; Strahl, R.; Kraus, T. High-Resolution Inkjet Printing of Quantum Dot Light-Emitting Microdiode Arrays. *Adv. Opt. Mater.* **2020**, *8*, 1901429.

(10) Zhang, C.; Wang, B.; Li, W.; Huang, S.; Kong, L.; Li, Z.; Li, L. Conversion of Invisible Metal-Organic Frameworks to Luminescent Perovskite Nanocrystals for Confidential Information Encryption and Decryption. *Nat. Commun.* **2017**, *8*, 1138.

(11) Liu, Y.; Zheng, Y.; Zhu, Y.; Ma, F.; Zheng, X.; Yang, K.; Zheng, X.; Xu, Z.; Ju, S.; Zheng, Y.; Guo, T.; Qian, L.; Li, F. Unclonable Perovskite Fluorescent Dots with Fingerprint Pattern for Multilevel Anticounterfeiting. *ACS Appl. Mater. Interfaces* **2020**, *12*, 39649−39656.

(12) Carro-Temboury, M. R.; Arppe, R.; Vosch, T.; Sørensen, T. J. An Optical Authentication System Based on Imaging of Excitation-Selected Lanthanide Luminescence. *Sci. Adv.* **2018**, *4*, e1701384.

(13) Kumar, P.; Nagpal, K.; Gupta, B. K. Unclonable Security Codes Designed from Multicolor Luminescent Lanthanide-Doped Y_2O_3 Nanorods for Anticounterfeiting. *ACS Appl. Mater. Interfaces* **2017**, *9*, 14301−14308.

(14) Gangwar, A. K.; Kanika; Kedawat, G.; Papanai, G. S.; Gupta, B. K. Single Excitable Dual Emissive Novel Luminescent Pigment to Generate Advanced Security Features for Anti-Counterfeiting Applications. *J. Mater. Chem. C* **2019**, *7*, 13867−13877.

(15) Gupta, B. K.; Kumar, P.; Dhar, A.; Aswal, D. K. Printable Bi-Luminescent Pigment for Security Ink Formulation and Process for the Preparation Thereof. U.S. Patent 20,190,111,724 A1, April 2019.

(16) Ramalho, J. F. C. B.; Correia, S. F. H.; Fu, L.; Dias, L. M. S.; Adão, P.; Mateus, P.; Ferreira, R. A. S.; André, P. S. Super Modules-Based Active QR Codes for Smart Trackability and IoT: A Responsive-Banknotes Case Study. *npj Flexible Electron.* **2020**, *4*, 11.

(17) You, M.; Zhong, J.; Hong, Y.; Duan, Z.; Lin, M.; Xu, F. Inkjet Printing of Upconversion Nanoparticles for Anti-Counterfeit Applications. *Nanoscale* **2015**, *7*, 4423−4431.

(18) Kalytchuk, S.; Wang, Y.; Poláková, K.; Zbořil, R. Carbon Dot Fluorescence-Lifetime-Encoded Anti-Counterfeiting. *ACS Appl. Mater. Interfaces* **2018**, *10*, 29902−29908.

(19) Jiang, K.; Wang, Y.; Gao, X.; Cai, C.; Lin, H. Facile, Quick, and Gram-Scale Synthesis of Ultralong-Lifetime Room-Temperature-Phosphorescent Carbon Dots by Microwave Irradiation. *Angew. Chem., Int. Ed.* **2018**, *57*, 6216−6220.

(20) Yang, J.-C.; Ho, Y.-C.; Chan, Y.-H. Ultrabright Fluorescent Polymer Dots with Thermochromic Characteristics for Full-Color Security Marking. *ACS Appl. Mater. Interfaces* **2019**, *11*, 29341−29349.

(21) Yan, L.; Yu, Y. Rapid and Eco-Friendly Synthesis of Red Fluorescent Gold Nanoclusters for Sensing and Anti-Counterfeiting Applications. *NANO* **2019**, *14*, 1950121.

(22) Häkkinen, H. Atomic and Electronic Structure of Gold Clusters: Understanding Flakes, Cages and Superatoms from Simple Concepts. *Chem. Soc. Rev.* **2008**, *37*, 1847−1859.
(23) Chakraborty, I.; Pradeep, T. Atomically Precise Clusters of Noble Metals: Emerging Link Between Atoms and Nanoparticles. *Chem. Rev.* **2017**, *117*, 8208−8271.
(24) Jin, R.; Zeng, C.; Zhou, M.; Chen, Y. Atomically Precise Colloidal Metal Nanoclusters and Nanoparticles: Fundamentals and Opportunities. *Chem. Rev.* **2016**, *116*, 10346−10413.
(25) Yao, Q.; Chen, T.; Yuan, X.; Xie, J. Toward Total Synthesis of Thiolate-Protected Metal Nanoclusters. *Acc. Chem. Res.* **2018**, *51*, 1338−1348.
(26) Yamazoe, S.; Koyasu, K.; Tsukuda, T. Nonscalable Oxidation Catalysis of Gold Clusters. *Acc. Chem. Res.* **2014**, *47*, 816−824.
(27) Li, G.; Jin, R. Atomically Precise Gold Nanoclusters as New Model Catalysts. *Acc. Chem. Res.* **2013**, *46*, 1749−1758.
(28) Lim, D. C.; Seo, B. Y.; Nho, S.; Kim, D. H.; Hong, E. M.; Lee, J. Y.; Park, S.-Y.; Lee, C.-L.; Kim, Y. D.; Cho, S. Emissive Nanoclusters Based on Subnanometer-Sized Au_{38} Cores for Boosting the Performance of Inverted Organic Photovoltaic Cells. *Adv. Energy Mater.* **2015**, *5*, 1500393.
(29) Abbas, M. A.; Yoon, S. J.; Kim, H.; Lee, J.; Kamat, P. V.; Bang, J. H. Ag(I)-Thiolate-Protected Silver Nanoclusters for Solar Cells: Electrochemical and Spectroscopic Look into the Photoelectrode/Electrolyte Interface. *ACS Appl. Mater. Interfaces* **2019**, *11*, 12492−12503.
(30) Koh, T.-W.; Hiszpanski, A. M.; Sezen, M.; Naim, A.; Galfsky, T.; Trivedi, A.; Loo, Y.-L.; Menon, V.; Rand, B. P. Metal Nanocluster Light-Emitting Devices with Suppressed Parasitic Emission and Improved Efficiency: Exploring the Impact of Photophysical Properties. *Nanoscale* **2015**, *7*, 9140−9146.
(31) Chao, Y.-C.; Cheng, K.-P.; Lin, C.-Y.; Chang, Y.-L.; Ko, Y.-Y.; Hou, T.-Y.; Huang, C.-Y.; Chang, W. H.; Lin, C.-A. J. Non-Toxic Gold Nanoclusters for Solution-Processed White Light-Emitting Diodes. *Sci. Rep.* **2018**, *8*, 8860.
(32) Mathew, A.; Sajanlal, P. R.; Pradeep, T. Selective Visual Detection of TNT at the Sub-Zeptomole Level. *Angew. Chem., Int. Ed.* **2012**, *51*, 9596−9600.
(33) Chen, T.-H.; Tseng, W.-L. (Lysozyme Type VI)-Stabilized Au_8 Clusters: Synthesis Mechanism and Application for Sensing of Glutathione in a Single Drop of Blood. *Small* **2012**, *8*, 1912−1919.
(34) Yue, Y.; Liu, T.-Y.; Li, H.-W.; Liu, Z.; Wu, Y. Microwave-Assisted Synthesis of BSA-Protected Small Gold Nanoclusters and Their Fluorescence-Enhanced Sensing of Silver(I) Ions. *Nanoscale* **2012**, *4*, 2251−2254.
(35) Yuan, X.; Luo, Z.; Yu, Y.; Yao, Q.; Xie, J. Luminescent Noble Metal Nanoclusters as an Emerging Optical Probe for Sensor Development. *Chem. - Asian J.* **2013**, *8*, 858−871.
(36) Muhammed, M. A. H.; Verma, P. K.; Pal, S. K.; Retnakumari, A.; Koyakutty, M.; Nair, S.; Pradeep, T. Luminescent Quantum Clusters of Gold in Bulk by Albumin-Induced Core Etching of Nanoparticles: Metal Ion Sensing, Metal-Enhanced Luminescence, and Biolabeling. *Chem. Eur. J.* **2010**, *16*, 10103−10112.
(37) Lin, C.-A. J.; Yang, T.-Y.; Lee, C.-H.; Huang, S. H.; Sperling, R. A.; Zanella, M.; Li, J. K.; Shen, J.-L.; Wang, H.-H.; Yeh, H.-I.; Parak, W. J.; Chang, W. H. Synthesis, Characterization, and Bioconjugation of Fluorescent Gold Nanoclusters Toward Biological Labeling Applications. *ACS Nano* **2009**, *3*, 395−401.
(38) Wu, X.; He, X.; Wang, K.; Xie, C.; Zhou, B.; Qing, Z. Ultrasmall near-Infrared Gold Nanoclusters for Tumor Fluorescence Imaging In Vivo. *Nanoscale* **2010**, *2*, 2244−2249.
(39) Shibu, E. S.; Sugino, S.; Ono, K.; Saito, H.; Nishioka, A.; Yamamura, S.; Sawada, M.; Nosaka, Y.; Biju, V. Singlet-Oxygen-Sensitizing Near-Infrared-Fluorescent Multimodal Nanoparticles. *Angew. Chem., Int. Ed.* **2013**, *52*, 10559−10563.
(40) Yu, Y.; New, S. Y.; Xie, J.; Su, X.; Tan, Y. N. Protein-Based Fluorescent Metal Nanoclusters for Small Molecular Drug Screening. *Chem. Commun.* **2014**, *50*, 13805−13808.
(41) Wang, Y.; Chen, J.; Irudayaraj, J. Nuclear Targeting Dynamic of Gold Nanoclusters for Enhanced Therapy of $HER2^+$ Breast Cancer. *ACS Nano* **2011**, *5*, 9718−9725.
(42) Zhang, X.-D.; Chen, J.; Luo, Z.; Wu, D.; Shen, X.; Song, S.-S.; Sun, Y.-M.; Liu, P.-X.; Zhao, J.; Huo, S.; Fan, S.; Fan, F.; Liang, X.-J.; Xie, J. Enhanced Tumor Accumulation of Sub-2 nm Gold Nanoclusters for Cancer Radiation Therapy. *Adv. Healthcare Mater.* **2014**, *3*, 133−141.
(43) Jadzinsky, P. D.; Calero, G.; Ackerson, C. J.; Bushnell, D. A.; Kornberg, R. D. Structure of a Thiol Monolayer-Protected Gold Nanoparticle at 1.1 Å Resolution. *Science* **2007**, *318*, 430−433.
(44) Jensen, K. M. O.; Juhas, P.; Tofanelli, M. A.; Heinecke, C. L.; Vaughan, G.; Ackerson, C. J.; Billinge, S. J. L. Polymorphism in Magic-Sized $Au_{144}(SR)_{60}$ Clusters. *Nat. Commun.* **2016**, *7*, 11859.
(45) Shichibu, Y.; Negishi, Y.; Tsunoyama, H.; Kanehara, M.; Teranishi, T.; Tsukuda, T. Extremely High Stability of Glutathionate-Protected Au_{25} clusters against Core Etching. *Small* **2007**, *3*, 835−839.
(46) Zhu, M.; Aikens, C. M.; Hollander, F. J.; Schatz, G. C.; Jin, R. Correlating the Crystal Structure of a Thiol-Protected Au_{25} Cluster and Optical Properties. *J. Am. Chem. Soc.* **2008**, *130*, 5883−5885.
(47) Joshi, C. P.; Bootharaju, M. S.; Alhilaly, M. J.; Bakr, O. M. $[Ag_{25}(SR)_{18}]^-$: The "Golden" Silver Nanoparticle. *J. Am. Chem. Soc.* **2015**, *137*, 11578−11581.
(48) Yang, H.; Wang, Y.; Huang, H.; Gell, L.; Lehtovaara, L.; Malola, S.; Häkkinen, H.; Zheng, N. All-Thiol-Stabilized Ag_{44} and $Au_{12}Ag_{32}$ Nanoparticles with Single-Crystal Structures. *Nat. Commun.* **2013**, *4*, 2422.
(49) Rival, J. V.; Nonappa; Shibu, E. S. Light-Triggered Reversible Supracolloidal Self-Assembly of Precision Gold Nanoclusters. *ACS Appl. Mater. Interfaces* **2020**, *12*, 14569−14577.
(50) Donkers, R. L.; Lee, D.; Murray, R. W. Synthesis and Isolation of the Molecule-like Cluster $Au_{38}(PhCH_2CH_2S)_{24}$. *Langmuir* **2004**, *20*, 1945−1952.
(51) Yu, Y.; Luo, Z.; Chevrier, D. M.; Leong, D. T.; Zhang, P.; Jiang, D.-e.; Xie, J. Identification of a Highly Luminescent $Au_{22}(SG)_{18}$ Nanocluster. *J. Am. Chem. Soc.* **2014**, *136*, 1246−1249.
(52) Shibu, E. S.; Pradeep, T. Quantum Clusters in Cavities: Trapped Au_{15} in Cyclodextrins. *Chem. Mater.* **2011**, *23*, 989−999.
(53) AbdulHalim, L. G.; Bootharaju, M. S.; Tang, Q.; Del Gobbo, S.; AbdulHalim, R. G.; Eddaoudi, M.; Jiang, D.-e.; Bakr, O. M. $Ag_{29}(BDT)_{12}(TPP)_4$: A Tetravalent Nanocluster. *J. Am. Chem. Soc.* **2015**, *137*, 11970−11975.
(54) You, M.; Lin, M.; Wang, S.; Wang, X.; Zhang, G.; Hong, Y.; Dong, Y.; Jin, G.; Xu, F. Three-Dimensional Quick Response Code Based on Inkjet Printing of Upconversion Fluorescent Nanoparticles for Drug Anti-Counterfeiting. *Nanoscale* **2016**, *8*, 10096−10104.
(55) Lopez, P.; Lara, H. H.; Mullins, S. M.; Black, D. M.; Ramsower, H. M.; Alvarez, M. M.; Williams, T. L.; Lopez-Lozano, X.; Weissker, H.-C.; García, A. P.; Garzón, I. L.; Demeler, B.; López-Ribot, J. L.; Yacamán, M. J.; Whetten, R. L. Tetrahedral (*T*) Closed-Shell Cluster of 29 Silver Atoms & 12 Lipoate Ligands, $[Ag_{29}(R\text{-}\alpha\text{-}LA)_{12}]^{(3-)}$: Antibacterial and Antifungal Activity. *ACS Appl. Nano Mater.* **2018**, *1*, 1595−1602.
(56) Wen, X.; Yu, P.; Toh, Y.-R.; Hsu, A.-C.; Lee, Y.-C.; Tang, J. Fluorescence Dynamics in BSA-Protected Au_{25} Nanoclusters. *J. Phys. Chem. C* **2012**, *116*, 19032−19038.
(57) Khatun, E.; Ghosh, A.; Chakraborty, P.; Singh, P.; Bodiuzzaman, M.; Ganesan, P.; Nataranjan, G.; Ghosh, J.; Pal, S. K.; Pradeep, T. A Thirty-Fold Photoluminescence Enhancement Induced by Secondary Ligands in Monolayer Protected Silver Clusters. *Nanoscale* **2018**, *10*, 20033−20042.
(58) Bootharaju, M. S.; Kozlov, S. M.; Cao, Z.; Harb, M.; Parida, M. R.; Hedhili, M. N.; Mohammed, O. F.; Bakr, O. M.; Cavallo, L.; Basset, J.-M. Direct *Versus* Ligand-Exchange Synthesis of $[PtAg_{28}(BDT)_{12}(TPP)_4]^{4-}$ Nanoclusters: Effect of a Single-Atom Dopant on the Optoelectronic and Chemical Properties. *Nanoscale* **2017**, *9*, 9529−9536.

https://dx.doi.org/10.1021/acsami.0c21127
ACS Appl. Mater. Interfaces 2021, 13, 10583−10593

(59) Kang, X.; Wang, S.; Zhu, M. Observation of a New Type of Aggregation-Induced Emission in Nanoclusters. *Chem. Sci.* **2018**, *9*, 3062−3068.
(60) Alhilaly, M. J.; Bootharaju, M. S.; Joshi, C. P.; Besong, T. M.; Emwas, A.-H.; Juarez-Mosqueda, R.; Kaappa, S.; Malola, S.; Adil, K.; Shkurenko, A.; Häkkinen, H.; Eddaoudi, M.; Bakr, O. M. $[Ag_{67}(SPhMe_2)_{32}(PPh_3)_8]^{3+}$: Synthesis, Total Structure, and Optical Properties of a Large Box-Shaped Silver Nanocluster. *J. Am. Chem. Soc.* **2016**, *138*, 14727−14732.
(61) Bandodkar, A. J.; Nuñez-Flores, R.; Jia, W.; Wang, J. All-Printed Stretchable Electrochemical Devices. *Adv. Mater.* **2015**, *27*, 3060−3065.
(62) Bandodkar, A. J.; Jeerapan, I.; You, J.-M.; Nuñez-Flores, R.; Wang, J. Highly Stretchable Fully-Printed CNT-Based Electrochemical Sensors and Biofuel Cells: Combining Intrinsic and Design-Induced Stretchability. *Nano Lett.* **2016**, *16*, 721−727.
(63) Liang, J.; Tong, K.; Pei, Q. A Water-Based Silver-Nanowire Screen-Print Ink for the Fabrication of Stretchable Conductors and Wearable Thin-Film Transistors. *Adv. Mater.* **2016**, *28*, 5986−5996.
(64) Rajendran, V.; Mohan, A. M. V.; Jayaraman, M.; Nakagawa, T. All-Printed, Interdigitated, Freestanding Serpentine Interconnects Based Flexible Solid State Supercapacitor for Self-Powered Wearable Electronics. *Nano Energy* **2019**, *65*, 104055.
(65) Chakraborty, P.; Nag, A.; Chakraborty, A.; Pradeep, T. Approaching Materials with Atomic Precision Using Supramolecular Cluster Assemblies. *Acc. Chem. Res.* **2019**, *52*, 2−11.
(66) Yahia-Ammar, A.; Sierra, D.; Mérola, F.; Hildebrandt, N.; Le Guével, X. Self-Assembled Gold Nanoclusters for Bright Fluorescence Imaging and Enhanced Drug Delivery. *ACS Nano* **2016**, *10*, 2591−2599.
(67) Chandra, S.; Nonappa; Beaune, G.; Som, A.; Zhou, S.; Lahtinen, J.; Jiang, H.; Timonen, J. V. I.; Ikkala, O.; Ras, R. H. A. Highly Luminescent Gold Nanocluster Frameworks. *Adv. Opt. Mater.* **2019**, *7*, 1900620.
(68) Mortensen, J. J.; Hansen, L. B.; Jacobsen, K. W. Real-Space Grid Implementation of the Projector Augmented Wave Method. *Phys. Rev. B* **2005**, *71*, 035109.
(69) Perdew, J. P.; Burke, K.; Ernzerhof, M. Generalized Gradient Approximation Made Simple. *Phys. Rev. Lett.* **1996**, *77*, 3865−3868.
(70) Humphrey, W.; Dalke, A.; Schulten, K. VMD: Visual Molecular Dynamics. *J. Mol. Graphics* **1996**, *14*, 33−38.

https://dx.doi.org/10.1021/acsami.0c21127
ACS Appl. Mater. Interfaces 2021, 13, 10583−10593